Valence-band satellite in the ferromagnetic nickel: LDA+DMFT study with exact diagonalization

Jindřich Kolorenč,[1,2,*] Alexander I. Poteryaev,[3,4] and Alexander I. Lichtenstein[1]

[1] *Institut für Theoretische Physik, Universität Hamburg, Jungiusstraße 9, D-20355 Hamburg, Germany*
[2] *Institute of Physics, Academy of Sciences of the Czech Republic, Na Slovance 2, CZ-182 21 Praha 8, Czech Republic*
[3] *Institute of Metal Physics, Russian Academy of Sciences, 620990 Ekaterinburg, Russia*
[4] *Institute of Quantum Materials Science, 620107 Ekaterinburg, Russia*

(Dated: March 1, 2012)

The valence-band spectrum of the ferromagnetic nickel is calculated using the LDA+DMFT method. The auxiliary impurity model emerging in the course of the calculations is discretized and solved with the exact diagonalization, or, more precisely, with the Lanczos method. Particular emphasis is given to spin dependence of the valence-band satellite that is observed around 6 eV below the Fermi level. The calculated satellite is strongly spin polarized in accord with experimental findings.

PACS numbers: 71.20.Be, 71.15.−m, 75.30.−m

I. INTRODUCTION

The electronic structure of transition metals has been intensively studied for a number of decades. Notwithstanding, certain aspects of the electron behavior in these materials are still not completely understood. Comparison of experimental findings with effective one-electron band theories have indicated that a more thorough treatment of quantum many-body effects is necessary to accurately describe the physical reality.

A prototypical metal displaying pronounced electron correlations is the ferromagnetic nickel, where the one-particle spectrum obtained using the local-density approximation (LDA) to the density-functional theory (DFT) noticeably departs from the spectra measured in photoemission experiments. The calculated $3d$ bandwidth as well as the exchange splitting are too large.[1,2] Moreover, the LDA completely misses the satellite feature located at approximately 6 eV below the Fermi level.[3–5] This satellite was originally attributed to plasmon excitations,[4] but an alternative view was soon proposed,[6,7] according to which the satellite is a result of a correlated state of two $3d$ holes localized in a single atom. The latter picture is supported by the observed resonant enhancement of the satellite, during which a second scattering channel involving $3p$ electrons and ending in the same two-hole final state becomes active.[8–10] The correspondence between the satellite and the localized two-hole states can be explicitly visualized in simplified finite-sized models that allow for an exact many-body solution.[11,12]

A more quantitative description of the electron correlations in nickel can be achieved by incorporating a selfenergy into the LDA or Hartree–Fock bandstructure.[13–15] Usually, the selfenergy is assumed local, that is, wavevector independent. The most sophisticated local selfenergy is provided by the dynamical-mean-field theory (DMFT)[16] that maps the problem of interacting lattice electrons onto an impurity model where the interactions are restricted to a single lattice site. The combination of LDA and DMFT (the so-called LDA+DMFT method) was applied to the electronic structure of nickel several times in the past, using different methods to solve the auxiliary impurity model.[17–21] A reasonable description was achieved employing the Hirsch–Fye quantum Monte Carlo (QMC) method as the impurity solver.[17] The QMC methods have many merits. In particular, they are consistently accurate regardless of the strength of correlations in the system. But they have weaknesses too. The QMC calculations of the one-particle spectral functions involve a numerical continuation from the imaginary time to the real frequencies, a procedure with a limited resolution especially at higher binding energies. Additionally, the QMC algorithm used in Ref. 17 is limited to a diagonal-only Coulomb interaction. This truncation breaks a subset of symmetries characterizing the full Coulomb operator, which can lead to undesirable side effects.

In this paper we solve the auxiliary impurity model of the LDA+DMFT by means of the Lanczos method. This strategy involves a discretization of the impurity model which represents an obvious limitation on the achievable accuracy. The sources of errors in this approach are, however, very different from those in the QMC method and the two impurity solvers can thus offer complementary information. Using the Lanczos method, the one-particle Green's function can be evaluated directly anywhere in the complex plane without resorting to any extrapolation. It is also straightforward to compare the full and truncated Coulomb operators, and we make this comparison in Sec. III.

II. METHOD

We start from the bare electronic structure of Ni expressed in terms of a tight-binding LMTO model[22] containing $4s$, $3d$ and $4p$ electronic states. The one-electron Hamiltonian $\hat{H}(\mathbf{k})$ is obtained as a solution of the local-

density approximation and the correlations beyond this approximation are accounted for by a local selfenergy $\hat{\Sigma}$ acting in the subspace of the d orbitals. The selfenergy is spin polarized whereas the Hamiltonian $\hat{H}(\mathbf{k})$ is spin independent. Taking $\hat{H}(\mathbf{k})$ from the spin-polarized LDA is also possible, although this route was found as less accurate earlier.[18]

The selfenergy $\hat{\Sigma}$ is constructed with the aid of an impurity model defined by a Hamiltonian $\hat{H}_{\mathrm{imp}} = \hat{H}^{(0)}_{\mathrm{imp}} + \hat{U}$ that describes a single d shell hybridized with a sea of auxiliary conduction electrons. These auxiliary electrons, often referred to as the bath, model the environment around the d shell in the actual nickel lattice. The Coulomb interaction $\hat{U}$ acts only among the d orbitals and the one-particle part $\hat{H}^{(0)}_{\mathrm{imp}}$ has the form

$$\hat{H}^{(0)}_{\mathrm{imp}} = \sum_{m\sigma} \epsilon_{m\sigma} \hat{d}^{\dagger}_{m\sigma} \hat{d}_{m\sigma} + \sum_{km\sigma} \epsilon_{km\sigma} \hat{c}^{\dagger}_{km\sigma} \hat{c}_{km\sigma} + \sum_{km\sigma} V_{km\sigma} \left(\hat{d}^{\dagger}_{m\sigma} \hat{c}_{km\sigma} + \hat{c}^{\dagger}_{km\sigma} \hat{d}_{m\sigma} \right), \quad (1)$$

where $\hat{d}^{\dagger}_{m\sigma}$ creates an electron in the d shell and $\hat{c}^{\dagger}_{km\sigma}$ creates a conduction electron in the bath. The index m runs over $e_g = \{x^2-y^2, z^2\}$ and $t_{2g} = \{xy, xz, yz\}$ states, and $\sigma \in \{\uparrow, \downarrow\}$ labels spin projections. The hybridization parameters $V_{km\sigma}$ couple only those impurity and bath levels that carry the same indices m and σ, and hence the cubic symmetry and the electron spins are preserved.

Provided we can solve the interacting impurity model, the sought for selfenergy $\hat{\Sigma}$ is obtained as

$$\hat{\Sigma} = \hat{G}^{-1}_{\mathrm{imp}}\big[\hat{H}^{(0)}_{\mathrm{imp}}\big] - \hat{G}^{-1}_{\mathrm{imp}}\big[\hat{H}_{\mathrm{imp}}\big], \quad (2a)$$

where $\hat{G}_{\mathrm{imp}}[\hat{H}]$ represents the Green's function matrix in the d-orbital subspace evaluated for a general impurity Hamiltonian $\hat{H}$. The matrix $\hat{G}_{\mathrm{imp}}\big[\hat{H}^{(0)}_{\mathrm{imp}}\big]$, which we will denote as $\hat{\mathcal{G}}$ for short, is usually referred to as the bath Green's function.

So far, we have not specified how the parameters entering the Hamiltonian $\hat{H}_{\mathrm{imp}}$ should be determined. The missing link to the original lattice electrons is provided by a condition

$$\hat{G}_{\mathrm{imp}}\big[\hat{H}_{\mathrm{imp}}\big] = \hat{G}\big[\hat{H}(\mathbf{k}), \hat{\Sigma}\big] \quad (2b)$$

that equates $\hat{G}_{\mathrm{imp}}$ to the local d-orbital Green's function $\hat{G}$ evaluated in the lattice. The right-hand side of Eq. (2b) can be expressed as a momentum sum over the first Brillouin zone

$$\hat{G}(z) = \frac{1}{N} \sum_{k} \big[(z+\mu)\hat{I} - \hat{H}(\mathbf{k}) - \hat{\Sigma}(z)\big]^{-1}, \quad (3)$$

where $\hat{I}$ stands for the identity operator and the chemical potential μ is chosen such that the $4s$-$3d$-$4p$ space holds ten electrons per Ni atom.

Equations (2) define the dynamical-mean-field approximation. They are iteratively solved for $\hat{\Sigma}$ and $\hat{H}^{(0)}_{\mathrm{imp}}$ while $\hat{H}(\mathbf{k})$ and $\hat{U}$ act as inputs. The most involved part of this procedure is the solution of the multi-orbital impurity model. A number of approximations of varied accuracy have been used to find this solution in the context of the DMFT. Here we discretize the impurity Hamiltonian $\hat{H}_{\mathrm{imp}}$ and then solve the resulting finite-sized cluster $\hat{H}_{\mathrm{c}}$ essentially exactly by means of the Lanczos method. This strategy was successfully applied to the DMFT equations for the repulsive[16,23] and attractive[24] single-band Hubbard models as well as for realistic multi-band problems.[25] The discretization $\hat{H}_{\mathrm{imp}} \to \hat{H}_{\mathrm{c}}$ amounts to a replacement of the infinite sums (integrals) over k in Eq. (1) with short finite sums. In our particular case, the index k takes only two values, that is, each impurity orbital is connected to just two bath orbitals.

The parameters of the discretized Hamiltonian ($\epsilon_{m\sigma}$, $\epsilon_{km\sigma}$ and $V_{km\sigma}$) are expressed as functions of $\hat{H}(\mathbf{k})$ and $\hat{\Sigma}$ with the aid of the relation

$$\hat{\mathcal{G}}^{-1}_{\mathrm{c}} \equiv \hat{G}^{-1}_{\mathrm{imp}}\big[\hat{H}^{(0)}_{\mathrm{c}}\big] \approx \hat{G}^{-1}\big[\hat{H}(\mathbf{k}), \hat{\Sigma}\big] + \hat{\Sigma} = \hat{\mathcal{G}}^{-1}, \quad (4)$$

which is just a rearranged form of Eqs. (2). At this point it is necessary to specify in what sense the discrete bath Green's function $\hat{\mathcal{G}}_{\mathrm{c}}$ approximates the continuous function $\hat{\mathcal{G}}$, that is, what is the precise meaning of the symbol $\approx$ in Eq. (4). It has become customary to minimize some distance between $\hat{\mathcal{G}}_{\mathrm{c}}(z)$ and $\hat{\mathcal{G}}(z)$ defined on the Matsubara frequencies $z = \mathrm{i}\omega_n$. A particularly convenient choice is a least-squares fit,[16,23–25] for instance

$$\min_{\substack{\epsilon_{m\sigma}, \epsilon_{km\sigma} \\ V_{km\sigma}}} \sum_{n} \left| \frac{1}{\mathcal{G}^{\mathrm{c}}_{m\sigma}(\mathrm{i}\omega_n)} - \frac{1}{\mathcal{G}_{m\sigma}(\mathrm{i}\omega_n)} \right|^2 \quad (5)$$

for each m and σ. For reasons that will be discussed later, we do not follow this fitting route but adopt an alternative approach instead. We obtain the parameters of the discretized Hamiltonian from the requirement of coincidence of the high-frequency asymptotics of $\hat{\mathcal{G}}_{\mathrm{c}}(z)$ and $\hat{\mathcal{G}}(z)$.[16,26]

The cluster Green's function $\hat{\mathcal{G}}_{\mathrm{c}}(z)$ can be written in an explicit form[27]

$$\mathcal{G}^{\mathrm{c}}_{m\sigma}(z) = \left(z - \epsilon_{m\sigma} - \sum_{k} \frac{V^2_{km\sigma}}{z - \epsilon_{km\sigma}} \right)^{-1} \quad (6)$$

whose expansion in powers of $1/z$ reads as

$$\mathcal{G}^{\mathrm{c}}_{m\sigma}(z) = \frac{1}{z} + \frac{\epsilon_{m\sigma}}{z^2} + \frac{\epsilon^2_{m\sigma} + \sum_k V^2_{km\sigma}}{z^3} + \frac{\epsilon^3_{m\sigma} + \sum_k V^2_{km\sigma}(\epsilon_{km\sigma} + 2\epsilon_{m\sigma})}{z^4} + \cdots \quad (7)$$

The continuous Green's function $\hat{\mathcal{G}}(z)$ can be expressed in terms of the density of states $g(z)$, and the coefficients of

the expansion in powers of $1/z$ are then given as moments of this density of states,

$$\mathcal{G}_{m\sigma}(z) = \int \frac{g_{m\sigma}(\epsilon)}{z-\epsilon}\,\mathrm{d}\epsilon = \sum_{n=1}^{\infty} \frac{1}{z^n} \underbrace{\int \epsilon^{n-1} g_{m\sigma}(\epsilon)\,\mathrm{d}\epsilon}_{M_{n-1}} . \quad (8)$$

With two bath orbitals per each impurity d orbital we have five parameters in $H_\mathrm{c}^{(0)}$ that carry the same indices m and σ, and thus we can match Eqs. (7) and (8) up to $1/z^6$.

We are mostly interested in the ground-state properties and in the one-particle spectrum in, say, the first 10 eV below the Fermi level. In the course of our calculations we observed that the discretization procedure defined by Eqs. (4)–(8) often placed some of the bath energies $\epsilon_{km\sigma}$ quite high above the Fermi level far outside the energy window of our interest. That by itself would not be an issue if it did not lead to an unphysical stabilization of a non-magnetic solution. (See Appendix B for an illustration and further discussion of the effect). In order to suppress this undesirable behavior, we modify the definition of the moments M_n to

$$M_n = \frac{\displaystyle\int_{\epsilon_l}^{\epsilon_u} \epsilon^n g_{m\sigma}(\epsilon)\,\mathrm{d}\epsilon}{\displaystyle\int_{\epsilon_l}^{\epsilon_u} g_{m\sigma}(\epsilon)\,\mathrm{d}\epsilon} . \quad (9)$$

The lower cutoff is a purely technical matter; it is set to $\epsilon_l = -9$ eV, that is, below the $4s$ band. The upper cutoff avoids the unphysical solution by not allowing the bath orbitals to drift to high energies. The results presented in Sec. III were obtained with $\epsilon_u = 2$ eV. The possibility to straightforwardly prevent the non-magnetic state with the aid of the upper cutoff ϵ_u is the main reason why we opted for the bath discretization by means of the $1/z$ expansion instead of the more frequently employed fitting on the Matsubara axis. We have not succeeded in finding a suitable modification of the fitting function, Eq. (5), that would reliably eliminate the non-magnetic solution.

The last component of the cluster Hamiltonian $\hat{H}_\mathrm{c}$ is the Coulomb interaction in the d shell. We use the spherically symmetric form

$$\hat{U} = \frac{1}{2} \sum_{\substack{mm'm''\\ m'''\sigma\sigma'}} U_{mm'm''m'''} \hat{d}^\dagger_{m\sigma} \hat{d}^\dagger_{m'\sigma'} \hat{d}_{m'''\sigma'} \hat{d}_{m''\sigma} - U_\mathrm{H} \sum_{m\sigma} \hat{d}^\dagger_{m\sigma} \hat{d}_{m\sigma} , \quad (10)$$

where the matrix $U_{mm'm''m'''}$ is parametrized by the Slater integrals $F_0 = 2$ eV, $F_2 = 8.2$ eV and $F_4 = 5.2$ eV. These numerical values correspond to Coulomb $U = 2$ eV and exchange $J = 0.95$ eV. The contribution to Eq. (10) proportional to U_H represents a rigid shift of the impurity levels downward, $\epsilon_{m\sigma} \to \epsilon_{m\sigma} - U_\mathrm{H}$, and accounts for the fact that the d–d Coulomb interactions are already partially included in the LDA Hamiltonian $\hat{H}(\mathbf{k})$ in the form of a static mean field. Several formulas have been proposed to express the Hartree-like double-counting potential U_H in terms of the occupation numbers of the d orbitals,[28–30] but we treat U_H as a free parameter similarly to Ref. 31, since neither of the standard choices leads to satisfactory results.

The need for "undressing" the LDA quasiparticles is one of the reasons why we prefer to build the many-body description on the top of the spin-restricted LDA bandstructure. If we started from polarized bands, the Hartree potential U_H would be polarized too, which would introduce an extra complexity to the problem. The double counting would have to be spin dependent also in the LDA+DMFT implementations that take into account the feedback of the selfenergy on $\hat{H}(\mathbf{k})$.[32,33]

Once the cluster Hamiltonian $\hat{H}_\mathrm{c}$ is fully specified, the one-particle Green's function $\hat{G}_\mathrm{c} \equiv \hat{G}_\mathrm{imp}[\hat{H}_\mathrm{c}]$ for individual d orbitals can be calculated. We employ the band Lanczos method[34,35] that allows for a simultaneous evaluation of all relevant matrix elements at once. Off-diagonal elements are directly accessible too, although this functionality is not used in the application at hand. For the purpose of the Lanczos method, $\hat{G}_\mathrm{c}$ is decomposed in the following form[36]

$$G^\mathrm{c}_{m\sigma}(z) = \frac{1}{Z}\left[G^{>}_{m\sigma}(z) + G^{<}_{m\sigma}(z)\right] , \quad (11)$$

where the two parts are

$$G^{>}_{m\sigma}(z) = \sum_\alpha \mathrm{e}^{-\beta E_\alpha} \langle\alpha|\hat{d}_{m\sigma}\big(z + E_\alpha - \hat{H}_\mathrm{c}\big)^{-1}\hat{d}^\dagger_{m\sigma}|\alpha\rangle ,$$
$$G^{<}_{m\sigma}(z) = \sum_\alpha \mathrm{e}^{-\beta E_\alpha} \langle\alpha|\hat{d}^\dagger_{m\sigma}\big(z - E_\alpha + \hat{H}_\mathrm{c}\big)^{-1}\hat{d}_{m\sigma}|\alpha\rangle .$$

The sums over the many-body eigenstates $|\alpha\rangle$, $\hat{H}_\mathrm{c}|\alpha\rangle = E_\alpha|\alpha\rangle$, represent grandcanonical averages with the chemical potential equal zero, and $Z = \sum_\alpha \mathrm{e}^{-\beta E_\alpha}$ stands for the corresponding partition function. The calculations are performed at low temperature $k_\mathrm{B}T = 1/\beta = 0.01$ eV so that only the ground state contributes to the sum over α most of the time. The eigenstate-eigenvalue pairs including all their degeneracies are found using the implicitly restarted Lanczos method as implemented in the ARPACK software package.[37]

III. RESULTS AND DISCUSSION

A. Ground-state properties

First we examine selected characteristics of the ground state and use them to estimate the double-counting potential U_H. Figure 1 shows the number of electrons in the d orbitals $n_d = n_{d\uparrow} + n_{d\downarrow}$ and the spin polarization of these orbitals $m_d = n_{d\uparrow} - n_{d\downarrow}$. The data calculated in the lattice and in the discretized impurity model are plotted side by side. They differ despite the DMFT iterations

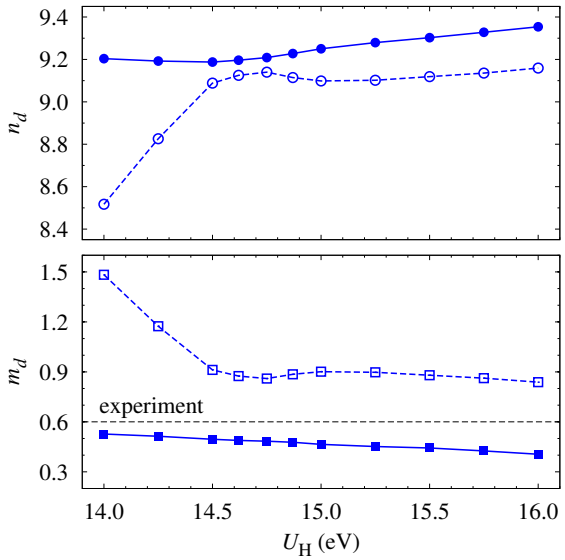

FIG. 1. (color online) The occupation of the d orbitals n_d (top) and the spin polarization m_d (bottom) plotted as functions of the double-counting potential $U_{\rm H}$. Empty symbols correspond to the cluster Green's function $\hat{G}_{\rm c}$, full symbols to the lattice Green's function $\hat{G}$.

being converged in the sense that the cluster Hamiltonian $H_{\rm c}$ no longer changed in the successive steps. The differences would vanish if we solved the full continuous impurity model, since Eq. (2b) would be exactly fulfilled in that case.

It turns out that n_d and m_d depend only weakly on the double-counting potential $U_{\rm H}$ when the latter is larger than approximately 14.5 eV. Below 14.5 eV the trend changes and the cluster quantities depart substantially from their lattice counterparts. Based on this observation we consider $U_{\rm H}$ below 14.5 eV as inappropriate. We note in passing that the double counting in the so-called fully localized limit[29,30] $U_{\rm H}^{\rm (FLL)} = U(n_d - 1/2) - J(n_d - 1)/2$ equals 13.2 eV for $n_d = 9$ and it is thus more than 1 eV too small to be applicable in our case. The so-called around mean-field form[28] of $U_{\rm H}$ provides an even smaller value.

The experimentally determined magnetization of the fcc nickel is approximately 0.6 $\mu_{\rm B}$ per atom.[38] Our calculations slightly underestimate this quantity even though the cluster solution, from which the spin-dependent self-energy is extracted, displays the maximal polarization characterized by $m_d = 5 - n_{d\downarrow}$.

The number of d electrons cannot be unambiguously defined in a solid and as such it does not represent a particularly useful measure of quality of our ground state. The d-band filling in nickel is often estimated as 9.4 per atom based on the measured magnetic moment and the assumption of the maximal d-shell polarization,[39] but reliability of this estimate is limited.

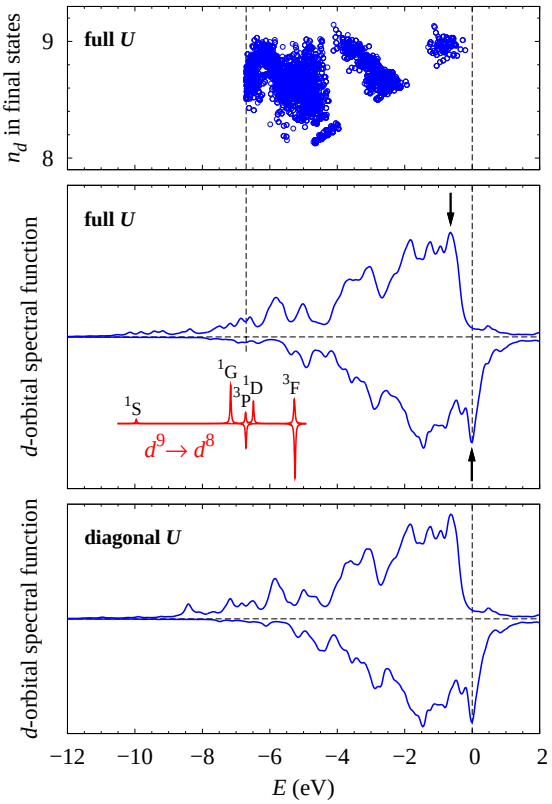

FIG. 2. (color online) Spin-resolved d-orbital spectral function of bulk Ni obtained with $U_{\rm H} = 15$ eV. The middle panel corresponds to the full Coulomb vertex, the bottom panel to the truncated vertex. The atomic $d^9 \rightarrow d^8$ transitions are displayed at an arbitrary scale and position in the middle panel for comparison with the shape of the satellite. The top panel shows the d-orbital occupation in the first 5000 many-body final states corresponding to the cluster Hamiltonian with the full vertex.

B. Valence-band spectrum

We find that the one-particle spectra corresponding to the double-counting potential $U_{\rm H}$ in the range 15.0 ± 0.5 eV are only barely distinguishable. Figure 2 shows the d-orbital spectral function $\mathrm{Im} \sum_m \big[G_{m\sigma}(E - \mathrm{i}0)\big]/\pi$ for $U_{\rm H} = 15$ eV. The calculated spectrum is relatively disappointing: the width of the main band (≈ 4 eV) as well as the exchange splitting are nearly identical to those obtained with the spin-polarized LDA, and thus share the same poor agreement with experiments. The symmetry-resolved exchange splitting at the Fermi level is given directly by the selfenergy and reads as

$$\Sigma_{e_g\uparrow}(E_{\rm F}) - \Sigma_{e_g\downarrow}(E_{\rm F}) \approx 0.3 \text{ eV}, \qquad (12a)$$

$$\Sigma_{t_{2g}\uparrow}(E_{\rm F}) - \Sigma_{t_{2g}\downarrow}(E_{\rm F}) \approx 0.8 \text{ eV}. \qquad (12b)$$

The d states near the Fermi level have predominantly the t_{2g} character, which results in the apparent exchange splitting of 0.6 eV that is visible as a shift between the top of the valence bands for the minority and majority

spins (indicated with arrows in Fig. 2). Appendix A indicates that the band width and the exchange splitting could possibly be improved if the impurity model was discretized using Eq. (5) instead of Eqs. (7) and (8), but, as discussed in Sec. II, that approach is not sufficiently reliable.

We identify the spectral features below -4.5 eV as the "6 eV satellite". It is strongly spin polarized in agreement with spin-resolved photoemission experiments.[40] In our calculations, the energy-integrated spectral weight is about three times larger for the majority spins than for the minority spins. Furthermore, the minority-spin states are located at reduced binding energies, which was also observed experimentally.[41] The calculated characteristics of the satellite corroborate its explanation based on transitions from the spin-polarized d^9 initial state to the d^8 final states. An illustration of such atomic spectral lines is added to Fig. 2 for comparison. The singlet final states ^{1}D, ^{1}G and ^{1}S exhibit a complete majority-spin polarization and lie deeper, the triplet states ^{3}F and ^{3}P carry a partial polarization in the opposite direction and lie shallower.

This simplified description of the satellite should not be taken too literally, however, at least not within our computational scheme. We have calculated the d-orbital occupation n_d corresponding to the final states in our discretized impurity model, the results are aligned with the lattice spectral function in Fig. 2. Although n_d indeed decreases as the binding energy increases, it is still considerably larger than eight in the satellite region where contributions from states with $n_d \geq 8.5$ are not an exception. This enhancement of n_d is due to impurity–bath hybridization as discussed at the end of Appendix B. It is possible that n_d is somewhat overestimated as a result of the sparse discretization of the bath.

As mentioned earlier, our calculations are rather insensitive to a choice of the potential U_{H} as long as it exceeds a threshold of approximately 14.5 eV. For smaller U_{H} the impurity orbitals in the cluster start to depopulate, which is accompanied by an increased intensity of the satellite. This result is in accord with experiments on alloys of Ni with electropositive metals.[42,43]

Finally, we compare spectral functions calculated with two versions of the Coulomb operator: the full spherically symmetric vertex discussed so far, and the diagonal-only vertex employed in the Hirsch–Fye QMC method.[17] Figure 2 shows that the simplification of the interaction has virtually no effect on the main d bands. The satellite, on the other hand, is visibly modified. The tail of the majority-spin spectrum does not extend as deep as with the full interaction, and the minority-spin satellite is shifted to smaller binding energies. It is possible that this slight shift in conjunction with the low resolution of the maximum-entropy method leads to a merger of the satellite with the main band for the minority spins, resulting in a fully spin-polarized satellite reported in Ref. 17.

IV. CONCLUSIONS

We have investigated the valence-band spectra of the ferromagnetic nickel within the LDA+DMFT framework. The auxiliary impurity model was discretized and then solved using the Lanczos method. The valence-band satellite and its spin dependence was reproduced in good agreement with spin-resolved photoemission experiments. The many-body renormalization of the $3d$ bands as well as the exchange splitting are found to be sensitive to the details of the bath discretization, which indicates that ten orbitals are probably not enough to approximate the bath to a satisfactory accuracy. The diagonalization method as employed in this paper is adequate for recovering features of atomic origin located at high binding energies but it is apparently too crude to capture the expected modification of the Fermi-liquid parameters at low binding energies.

ACKNOWLEDGMENTS

Financial support by the Deutsche Forschungsgemeinschaft through FOR 1346 is gratefully acknowledged. J. K. acknowledges financial support by the Alexander von Humboldt Foundation. A. P. acknowledges the Russian Foundation for Basic Research (Projects Nos. 10-02-00046, 10-02-91003, and 11-02-01443).

Appendix A: Comments on the bath discretization

In this appendix we return to the bath discretization using the least-squares fit of the bath Green's function with the functional form of Eq. (6) at the Matsubara frequencies. In the case of five orbitals in the bath, the self-consistent LDA+DMFT calculations are very stable and the resulting spectral function is shown in the Fig. 3. Although the satellite at high binding energies is not described as well as previously (Fig. 2), the renormalization of the main valence band and the exchange splitting come out as more reasonable. The width of the valence band is approximately 3 eV and the exchange spitting is about 0.3 eV, both of which are close to the photoemission experiments.[1,2] The fitting at the Matsubara frequencies is more sensitive to the behavior near the Fermi level than the method of moments, Eqs. (7) and (8), and hence it gives a finer control over the low-energy spectral features. Unfortunately, due to the effects discussed in the next appendix, it is not easy to converge the calculations to the correct state for ten orbitals in the bath. Nevertheless, we believe that it will eventually be possible to find an optimal way of fitting the bath Green's function that would lead to a reasonable description of both low- and high-energy parts of the spectrum simultaneously.

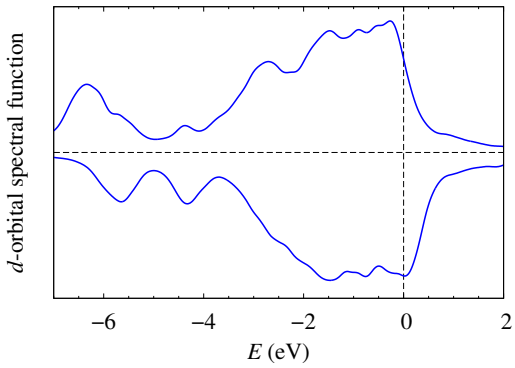

FIG. 3. (color online) Spin-resolved d-orbital spectral function of bulk Ni that was obtained with the bath discretized using the least-squares fit at the Matsubara frequencies (five orbitals in the bath).

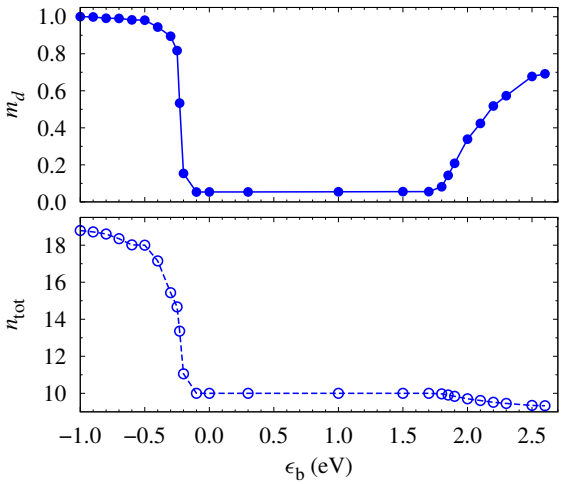

FIG. 4. (color online) Spin polarization of the d shell m_d (top) and the total number of electrons in the whole cluster $n_{\rm tot}$ (bottom) as functions of the bath-level position $\epsilon_{\rm b}$.

Appendix B: Magnetism in the finite cluster

Here we take a closer look at the issues that necessitated the introduction of the cutoffs in Eq. (9). To illustrate the problem, we use a simpler impurity model than that employed in Sec. III—we reduce the cluster to contain only one bath orbital per each impurity orbital and we assume spherical instead of cubic symmetry. Furthermore, we implement the Hamiltonian parameters used in Ref. 12, which gives us the opportunity to relate our calculations to this earlier study of electron correlations in nickel. The Slater integrals are $F_0 = 3.5$ eV, $F_2 = 9.79$ eV and $F_4 = 6.08$ eV, and the impurity–bath hopping is $V_{km\sigma} = 0.7$ eV. The bath-level position $\epsilon_{km\sigma} \equiv \epsilon_{\rm b}$ is treated as a free parameter and the double-counting potential $U_{\rm H}$ is determined such that there are always nine electrons in the impurity d orbitals. The temperature is $k_{\rm B}T = 0.01$ eV as before.

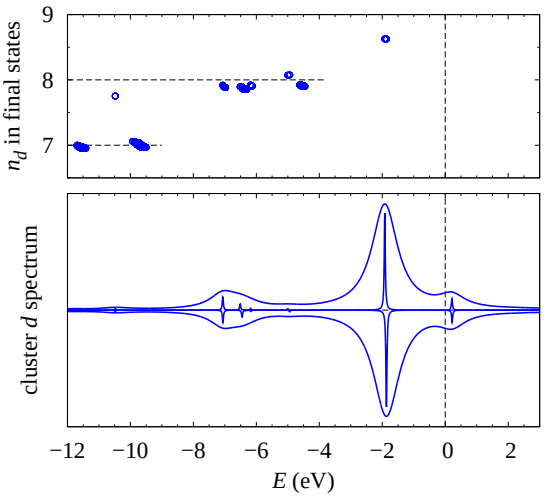

FIG. 5. (color online) Spin-resolved d-orbital spectral function of a cluster with parameters taken from Ref. 12 and $\epsilon_{\rm b} = 0$ eV (lower panel). The "envelope" is calculated with a large Lorentz broadening of 0.5 eV. The top panel shows the d-orbital occupation in the final states.

The spin polarization of the impurity orbitals is induced by a small magnetic field B coupled to the impurity spins. The coupling is described by an extra term in the cluster Hamiltonian,

$$\hat{H}_{\rm c}^{(B)} = \frac{B}{2} \sum_m \left(\hat{d}^\dagger_{m\uparrow} \hat{d}_{m\uparrow} - \hat{d}^\dagger_{m\downarrow} \hat{d}_{m\downarrow} \right) . \qquad \text{(B1)}$$

The resulting polarization is plotted in Fig. 4 as a function of the bath position $\epsilon_{\rm b}$ scanned across the Fermi level. The total number of electrons in the cluster is shown as well.

When the bath orbitals are sufficiently deep below the Fermi level, the bath is nearly full and a local magnetic moment is formed on the impurity. As the bath orbitals move up toward the Fermi level, the bath relatively quickly depopulates until it holds only a single electron. This electron, together with the other nine sitting in the impurity orbitals, forms a non-magnetic d^{10} closed shell. This state then remains stable even when the bath is raised relatively high above the Fermi level. Only for $\epsilon_{\rm b} > 2.4 V_{km\sigma} \approx 1.7$ eV the bath starts releasing the last electron and a magnetic ground state is restored. The larger cluster corresponding to our actual DMFT calculations shows an analogous behavior, only the non-magnetic solution occurs for 20 electrons in the cluster as there is an extra fully occupied shell of bath orbitals located deeper below the Fermi level.

It is clear that the non-magnetic solution does not correctly describe the d shell and its environment in the ferromagnetic nickel. Elevating the bath orbitals high above the Fermi level in order to support a magnetic ground state does not look as very plausible. This leaves us with the configuration where the bath states are nearly fully occupied and hence they model the nearly full d

orbitals of the nickel atoms surrounding the "impurity" site. To prevent the cluster Hamiltonian to enter the non-realistic regimes in the course of the DMFT iterations, we have introduced the upper cutoff ϵ_u in the integrals in Eq. (9). This cutoff does not allow the bath orbitals to drift too high and to lock into the non-magnetic solution.

It is instructive to compare the spectral functions corresponding to the different cluster ground states. Figure 5 shows the spectrum obtained when the bath orbitals are placed exactly at the Fermi level, $\epsilon_b = 0$. The local moment induced by the external magnetic field is negligible in this case and the spectral function is nearly symmetric. The spectrum is practically identical to the result presented in Ref. 12 as it should be, since we used the same parameters. The superimposed plot of the d-orbital filling n_d in the photoemission final states indicates that the satellite structures around -6.5 eV and near -10 eV are due to the d^8 final states.

The spectral function corresponding to the bath orbitals lowered to -0.4 eV is plotted in Fig. 6. The "6 eV satellite" has now a shape similar to our DMFT solution (Fig. 2) as well as to the experimental data: the minority-spin component is less intense and is located at smaller binding energies. Comparison of Figs. 5 and 6 reveals that the composition of the final states constituting the main d band is shifted toward a larger average n_d, likely due to an increased impurity–bath hybridization caused by the reduced distance between the impurity and bath orbitals. Analogously, the enhanced values $n_d \sim 8.5$ at the satellite in the DMFT solution (Fig. 2) are probably due to the hybridization with the extra shell of bath orbitals not present in the model discussed in this appendix.

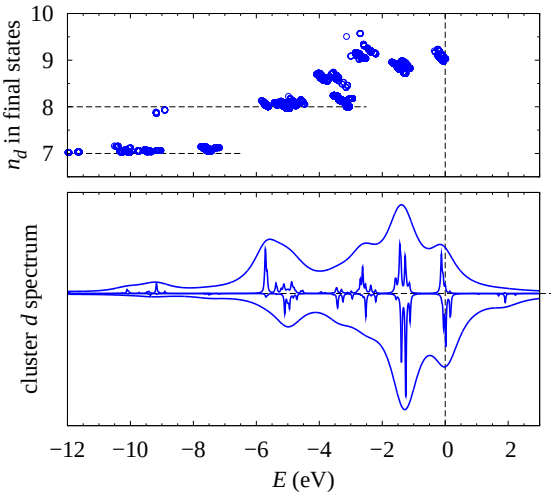

FIG. 6. (color online) Spectrum of the same model as Fig. 5, but with the bath orbitals shifted to -0.4 eV. The ground state is magnetic in this case. Note the different range of the top panel compared to Fig. 5.

* kolorenc@fzu.cz

[1] D. E. Eastman, F. J. Himpsel, and J. A. Knapp, Phys. Rev. Lett. **40**, 1514 (1978).
[2] W. Eberhardt and E. W. Plummer, Phys. Rev. B **21**, 3245 (1980).
[3] C. S. Fadley and D. A. Shirley, Phys. Rev. Lett. **21**, 980 (1968).
[4] Y. Baer, P. F. Hedén, J. Hedman, M. Klasson, C. Nordling, and K. Siegbahn, Solid State Commun. **8**, 517 (1970).
[5] S. Hüfner and G. K. Wertheim, Phys. Lett. A **47**, 349 (1974).
[6] S. Hüfner and G. K. Wertheim, Phys. Lett. A **51**, 299 (1975).
[7] P. C. Kemeny and N. J. Shevchik, Solid State Commun. **17**, 255 (1975).
[8] C. Guillot, Y. Ballu, J. Paigné, J. Lecante, K. P. Jain, P. Thiry, R. Pinchaux, Y. Pétroff, and L. M. Falicov, Phys. Rev. Lett. **39**, 1632 (1977).
[9] L. A. Feldkamp and L. C. Davis, Phys. Rev. Lett. **43**, 151 (1979).
[10] R. Clauberg, W. Gudat, E. Kisker, E. Kuhlmann, and G. M. Rothberg, Phys. Rev. Lett. **47**, 1314 (1981).
[11] R. H. Victora and L. M. Falicov, Phys. Rev. Lett. **55**, 1140 (1985).
[12] A. Tanaka, T. Jo, and G. A. Sawatzky, J. Phys. Soc. Jpn. **61**, 2636 (1992).
[13] D. R. Penn, Phys. Rev. Lett. **42**, 921 (1979).
[14] A. Liebsch, Phys. Rev. Lett. **43**, 1431 (1979).
[15] J. Igarashi, P. Unger, K. Hirai, and P. Fulde, Phys. Rev. B **49**, 16181 (1994).
[16] A. Georges, G. Kotliar, W. Krauth, and M. J. Rozenberg, Rev. Mod. Phys. **68**, 13 (1996).
[17] A. I. Lichtenstein, M. I. Katsnelson, and G. Kotliar, Phys. Rev. Lett. **87**, 067205 (2001).
[18] M. I. Katsnelson and A. I. Lichtenstein, Eur. Phys. J. B **30**, 9 (2002).
[19] J. Braun, J. Minár, H. Ebert, M. I. Katsnelson, and A. I. Lichtenstein, Phys. Rev. Lett. **97**, 227601 (2006).
[20] A. Grechnev, I. Di Marco, M. I. Katsnelson, A. I. Lichtenstein, J. Wills, and O. Eriksson, Phys. Rev. B **76**, 035107 (2007).
[21] D. Benea, J. Minár, L. Chioncel, S. Mankovsky, and H. Ebert, Phys. Rev. B **85**, 085109 (2012).
[22] O. K. Andersen, Phys. Rev. B **12**, 3060 (1975).
[23] M. Caffarel and W. Krauth, Phys. Rev. Lett. **72**, 1545 (1994).
[24] A. Privitera, M. Capone, and C. Castellani, Phys. Rev. B **81**, 014523 (2010).
[25] C. A. Perroni, H. Ishida, and A. Liebsch, Phys. Rev. B **75**, 045125 (2007).
[26] Q. Si, M. J. Rozenberg, G. Kotliar, and A. E. Ruckenstein, Phys. Rev. Lett. **72**, 2761 (1994).
[27] A. C. Hewson, *The Kondo Problem to Heavy Femions* (Cambridge University Press, 1993).
[28] V. I. Anisimov, J. Zaanen, and O. K. Andersen, Phys. Rev. B **44**, 943 (1991).
[29] M. T. Czyżyk and G. A. Sawatzky, Phys. Rev. B **49**, 14211 (1994).

[30] I. V. Solovyev, P. H. Dederichs, and V. I. Anisimov, Phys. Rev. B **50**, 16861 (1994).
[31] M. Karolak, G. Ulm, T. Wehling, V. Mazurenko, A. Poteryaev, and A. Lichtenstein, J. Electron Spectrosc. Relat. Phenom. **181**, 11 (2010).
[32] A. B. Shick, J. Kolorenč, A. I. Lichtenstein, and L. Havela, Phys. Rev. B **80**, 085106 (2009).
[33] K. Haule, C.-H. Yee, and K. Kim, Phys. Rev. B **81**, 195107 (2010).
[34] A. Ruhe, Math. Comput. **33**, 680 (1979).
[35] H.-D. Meyer and S. Pal, J. Chem. Phys. **91**, 6195 (1989).
[36] M. Capone, L. de' Medici, and A. Georges, Phys. Rev. B **76**, 245116 (2007).
[37] R. B. Lehoucq, D. C. Sorensen, and C. Yang, *ARPACK Users' Guide* (SIAM, 1998).
[38] H. Danan, A. Herr, and A. J. P. Meyer, J. Appl. Phys. **39**, 669 (1968).
[39] N. F. Mott, Adv. Phys. **13**, 325 (1964).
[40] A. K. See and L. E. Klebanoff, Phys. Rev. B **51**, 11002 (1995).
[41] A. Kakizaki, K. Ono, K. Tanaka, K. Shimada, and T. Sendohda, Phys. Rev. B **55**, 6678 (1997).
[42] J. Fuggle and Z. Zolnierek, Solid State Commun. **38**, 799 (1981).
[43] J. C. Fuggle, F. U. Hillebrecht, R. Zeller, Z. Zołnierek, P. A. Bennett, and C. Freiburg, Phys. Rev. B **27**, 2145 (1983).